





Cite this: *Nanoscale*, 2025, **17**, 20089

## A metallosupramolecular-based ring-in-ring complex showing reversible host–guest dynamics and switchable electrochemical properties†

Joel Martínez-Visiedo,<sup>a</sup> Susana Ibáñez,<sup>a</sup> \*<sup>a</sup> Louise N. Dawe<sup>b</sup> and Eduardo Peris \*<sup>a</sup>

Studying reversible host–guest interactions is essential for developing flexible, efficient, and sustainable systems, as they enhance reusability, improve efficiency, and provide valuable insights for designing advanced materials and technologies. In this work, we describe the synthesis of a pyrene–naphthalenediimide-based heterocyclophane, which can be encapsulated in an iridium-cornered nanosized metallobox with a high binding affinity. Electrochemical studies of the resulting host–guest complex reveal that encapsulation significantly alters the cyclophane’s redox behavior, with the processes being highly sensitive to guest uptake and release dynamics. Reduction of the cyclophane occurs at the naphthalenediimide (NDI) unit, generating a radical species that is stabilized upon encapsulation within the metallobox cavity. Host–guest dynamics were investigated using variable temperature <sup>1</sup>H NMR spectroscopy, and the release and uptake of the guest can be precisely controlled by adding chloride or silver(I) ions. We believe that our studies can help the development of methodologies to controllably allow the release and uptake of guests from metallosupramolecular assemblies, which are central to many of the applications of these systems.

Received 30th June 2025,  
Accepted 23rd July 2025

DOI: 10.1039/d5nr02758f

rsc.li/nanoscale

### Introduction

Charge transfer (CT) complexes formed through  $\pi$ -stacking interactions between  $\pi$ -electron donors (D) and acceptors (A) have received significant attention in recent decades, because their inherent conducting properties make them particularly suitable for the development of well-defined nanostructures that hold promise as key components in the development of future electronic nanodevices.<sup>1</sup> Among these CT complexes, those based on the naphthalenediimide–pyrene system are of particular interest. The exceptional geometric compatibility between naphthalenediimide (NDI) and pyrene (Pyr) maximizes

the contact area between the two planar units, fostering strong interactions that are crucial for the design of nanodevices with remarkable optoelectronic properties.<sup>2</sup> The precise composition and packing structure of the NDI/Pyr mixture are critical for the development of materials with CT properties with the potential to be used in applications of multifunctional optoelectronic or photochemical devices. One of the most widely used strategies to build NDI–Pyr assemblies consists of the mixing of the NDI- and pyrene-based subcomponents, forming mixed stacked nanoassemblies in which the donors and acceptors occupy alternating positions (–ADAD–) along the  $\pi$ -stacking direction.<sup>3</sup> This strategy is designed to obtain CT functional materials from independent components through noncovalent bonds, therefore avoiding the harsh reaction conditions that are often utilized in chemical bond synthesis.<sup>4</sup> Although knowing the precise composition and packing structure of the CT complex is crucial, in most of the studies the optimal D/A ratio for an effective CT material remains unclear.<sup>5</sup> Another strategy to facilitate the precise control of D/A interactions is to use hollow supramolecular assemblies, so that the D/A units can preorganize by encapsulation enabling their interaction with each other.<sup>6</sup> Receptors capable of intercalating multiple stacks are very challenging,<sup>7</sup> because enabling well-defined discrete  $\pi$ -stacks can facilitate the study of the charge transport at the molecular level, a critical issue for the design of nanoscale electronic devices.<sup>8</sup>

<sup>a</sup>Institute of Advanced Materials (INAM). Centro de Innovación en Química Avanzada (ORFEO-CINQA), Universitat Jaume I, Av. Vicente Sos Baynat s/n, Castellón, E-12071, Spain. E-mail: maella@uji.es, eperis@uji.es

<sup>b</sup>Department of Chemistry and Biochemistry, Wilfrid Laurier University, 75 University Avenue West, Waterloo, Ontario, N2L 3C5, Canada

†Electronic supplementary information (ESI) available: Experimental details dealing with the characterization, calculation of binding affinities and X-ray diffraction details. This includes all NMR spectra, and description of methods for determining the association constants, observed kinetic constants and thermodynamic parameters. The file also contains the data related to the crystallographic studies. CCDC 2464529 and 2464533. For ESI and crystallographic data in CIF or other electronic format see DOI: <https://doi.org/10.1039/d5nr02758f>



Using a nanosized di-N-heterocyclic carbene (NHC) ligand, we recently synthesized two distinct iridium(III)-based metallorectangles, each supported by pyrazine<sup>9</sup> and 4,4'-bipyridine<sup>10</sup> ligands acting as structural pillars (labeled **1** and **2** in Scheme 1). The “shallow” pyrazine-supported metallorectangle successfully encapsulated a single planar guest in its cavity,<sup>9</sup> while the “deeper” bipyridine-based structure was capable of trapping pairs of planar guests in a cooperative manner,<sup>10</sup> thereby facilitating the formation of discrete quadruple stacks. These quadruple stacks were thermodynamically favored when donor/acceptor (D/A) heteroguests, such as NDI and coronene, were employed.

We hypothesized that incorporating a donor/acceptor (D/A)-containing cyclophane into the system would promote the formation of well-defined  $\pi$ -stacked complexes with metallobox **2**. The use of a cyclophane was expected to reduce the entropic penalty compared to introducing D/A guests separately. Additionally, we sought to exploit the shape of the metallobox cavity to investigate dynamic processes involving the relative motion of the guest within the host. Understanding such dynamic behavior is fundamental to the design of more complex molecular motions, which underpin the development of molecular machines. To test these hypotheses, we demonstrate that metallobox **2** efficiently encapsulates a newly synthesized NDI-pyrene cyclophane with high binding affinity. We further characterize the resulting host-guest complex, examining its charge-transfer (CT) properties and dynamic behavior.



**Scheme 1** Two nanosized metallorectangles built with a Janus quinoxalinophenanthrophenazine-bis-imidazolylidene ligand.

## Results and discussion

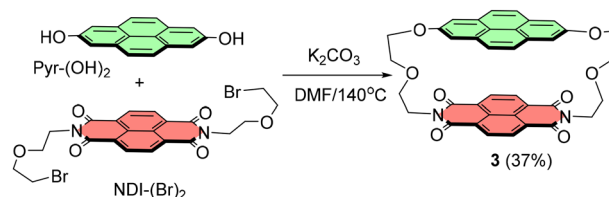
The NDI-pyrene cyclophane **3** was obtained by direct reaction between 2,7-dihydroxypyrene [Pyr-(OH)<sub>2</sub>] and *N,N'*-(bis(2-bromoethoxy)ethanol)-1,4,5,8-naphthalenediimide (NDI-Br<sub>2</sub>) in the presence of K<sub>2</sub>CO<sub>3</sub> in DMF, as depicted in Scheme 2. The resulting red solid was characterized by NMR spectroscopy and gave satisfactory elemental analysis.

The cyclic voltammetry of compound **3** shows two reversible redox events at  $E_{1/2}$  values of  $-1.15$  and  $-1.53$  V, which correspond to the sequential one-electron reduction of the NDI unit of the cyclophane to NDI<sup>•-</sup> and NDI<sup>2-</sup> (see Fig. 3 and ESI† for details). These redox potentials of **3** are 140 and 112 mV more negative than the related first and second redox potentials of NDI-(Br)<sub>2</sub> ( $E_{1/2} = -1.01$  V and  $-1.41$  V). This change may be ascribed to the CT interaction between the NDI and pyrene units of **3**.

The UV-vis spectrum of **3** in dichloromethane shows a very broad and structureless band at 490 nm, which is assigned to a CT transition. In the short-wavelength region of the spectrum vibrationally-resolved bands are observed, due to the NDI and pyrene components of the cyclophane.

The molecular structure of compound **3** features pyrene and NDI units connected by two 2-(2-ethoxyethoxy) linkers. These aromatic moieties adopt a parallel-displaced stacking configuration, with a centroid-to-centroid offset of 2.02 Å. The angle between their principal molecular axes is 13.36°, and the average interplanar distance between the NDI and pyrene units is 3.52 Å (Fig. 1).

Equimolar mixtures of **2** and **3** in CD<sub>2</sub>Cl<sub>2</sub> resulted in the quantitative formation of the related host: guest complex **3@2**, thus indicating a large binding affinity. The diffusion ordered spectroscopy (DOSY) spectrum of **3@2**, shows that the two sub-components of this molecular assembly have the same diffusion coefficient ( $4.37 \times 10^{-10} \text{ m}^2 \text{ s}^{-1}$ ), which is smaller than the coefficients found for the free molecules **2** and **3** (see ESI† for details), in agreement with the larger size that is expected for **3@2**. By using the Stokes-Einstein equation, these coefficients provide estimated hydrodynamic radii of 11.4 and 12.18 Å for **2** and **3@2**, respectively. Fig. 2 shows the aromatic region of the <sup>1</sup>H NMR spectrum (CD<sub>2</sub>Cl<sub>2</sub>) of **2**, **3** and **3@2**, from which a clear evidence of the efficiency of the complexation can be observed. As can be observed from the spectrum of **3@2**, all the resonances due to the pyrene and NDI units of the guest (f, g, e) are considerably shielded and, consequently, they show a considerable upfield shift compared to



**Scheme 2** Synthesis of the NDI-Pyr cyclophane **3**.



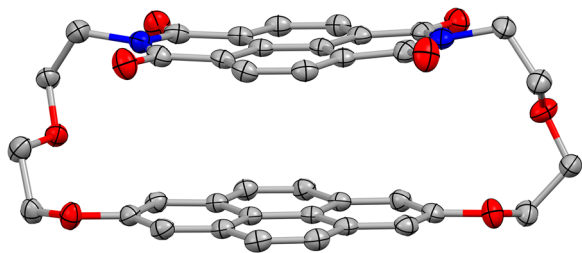


**Fig. 1** Molecular structure of the NDI-pyrene cyclophane **3** determined by X-ray diffractometry studies. Hydrogen atoms have been omitted for clarity. Carbon atoms are in grey, nitrogen in blue, and oxygen in red.

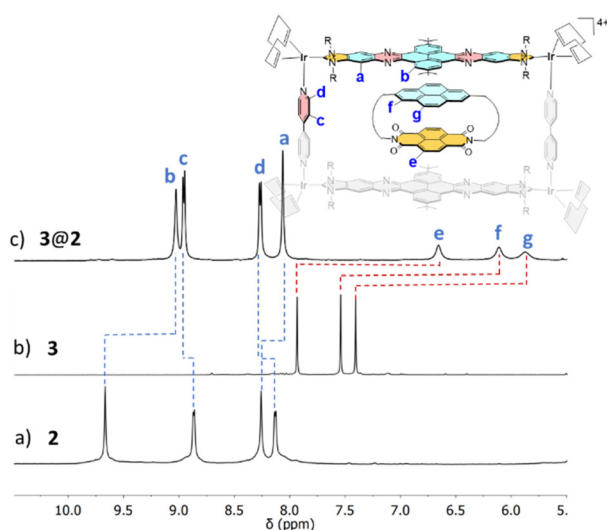


**Fig. 2** Selected region of the  $^1\text{H}$  NMR spectrum ( $\text{CD}_2\text{Cl}_2$ , 500 MHz, 298 K) of (a) **2**, (b) **3** and (c) **3@2**.

the resonances in the free guest. In addition, the complexation results in the upfield shift of the signals due to the aromatic protons of the di-NHC ligand (a, b), together with the downfield shift of the protons due to the bipyridine ligand of the host (d, c).

Single crystals of **3@2** suitable for X-ray diffraction studies were obtained by slow diffusion of hexane into a solution of the complex in tetrachloroethane (Fig. 3). The molecular structure consists of a tetra-iridium rectangle featuring two cofacial quinoxalinophenanthrophenazine-bis-imidazolyliene ligands and two 4,4'-bipyridine ligands, which form the long and short sides of the rectangle, respectively. One molecule of the heterocyclophane **3** is encapsulated within the host structure and resides in the central part of the cavity. Two orientations of the guest cyclophane are observed in the crystal structure, each with 50% occupancy. This dual occupancy arises from the asymmetric nature of the guest, which allows either the NDI or pyrene units to face either of the polyaromatic cores of the two bis-imidazolyliene ligands. The two orientations are related by inversion symmetry. Refinement details have been included in the ESI.† This configuration is consistent with variable-



**Fig. 3** Two perspectives of the molecular structure of **3@2** obtained from single X-ray diffraction studies. A single orientation of **3** is shown, and hydrogen atoms omitted from the figure for clarity. Counter anions ( $\text{BF}_4^-$ ) and solvent molecules were excluded from the model using a solvent mask. Carbon atoms are in blue, nitrogen atoms in red, oxygen atoms in green and iridium atoms in yellow.

temperature  $^1\text{H}$  NMR experiments described below, which reveal two degenerate configurations in equilibrium in solution. The Ir...Ir distance bridged by the di-NHC ligands is 22.57 Å, while the Ir...Ir distance across the bipyridine ligands measures 11.24 Å. The distances between the plane of the central pyrene unit of the host's di-NHC ligand and the NDI and pyrene units of the guest are 3.28 and 3.44 Å, respectively, indicating significant  $\pi$ - $\pi$  stacking interactions between the guest and host aromatic systems. The average interplanar distance between the NDI and pyrene units of the guest cyclophane is 3.51 Å, closely matching the value observed in the free cyclophane. Finally, the angle between the principal axes of the pyrene and NDI units of the guest is 12.87°. These two latter parameters indicate minimal distortion of the guest upon encapsulation.

We next carried out titration experiments in order to get information about the binding affinity between metallobox **2** and cyclophane **3**. The  $^1\text{H}$  NMR titration in  $\text{CD}_2\text{Cl}_2$  showed that the addition of increasing amounts of **3**, induced the upfield shift of the two resonances assigned to the protons of the polyaromatic linker of the di-NHC ligand, together with the downfield shift of the two signals due to the protons of the bipyridine ligand (see ESI† for full details). The titration showed that the encapsulating process shows fast kinetics on the NMR timescale, as only averaged resonances of **2** and **3@2** are observed. By using a global nonlinear regression analysis,<sup>11</sup>



we found that the data were best fitted to a 1 : 1 stoichiometric model, with an association constant of  $(2.4 \pm 0.2) \times 10^4 \text{ M}^{-1}$ .

Isothermal titration calorimetry (ITC) experiments were conducted to further investigate the interaction between metallobox **2** and cyclophane **3**. Titrations were carried out in chloroform by sequentially adding small aliquots of a 1 mM solution of **3** to a 0.18 mM solution of **2** in the calorimetric cell. The resulting data were best fitted to a one-site binding model, consistent with a 1 : 1 stoichiometry, yielding a binding constant of  $(2.0 \pm 0.6) \times 10^4 \text{ M}^{-1}$ . This value closely matches that obtained from the  $^1\text{H}$  NMR titrations. The enthalpy change ( $\Delta H$ ) for the binding event was determined to be  $-6.7 \pm 0.8 \text{ kcal mol}^{-1}$ , while the entropy change ( $\Delta S$ ) was  $-3.3 \text{ cal mol}^{-1} \text{ K}^{-1}$ . These thermodynamic parameters indicate that the encapsulation process is primarily enthalpically driven, with minimal entropic contribution.

We wanted to compare the redox behavior of **3** with that of **3@2** in order to garner information about the effects that the encapsulation may have in the electrochemical properties of the guest. As can be observed in Fig. 4a, the cyclic voltammetry of **3@2** shows two redox events that can be related to the one-electron and two-electron sequential reductions of the NDI unit of the guest. When cyclic voltammetry (CV) is performed at a scan rate of  $100 \text{ mV s}^{-1}$ , the first reduction of the host-guest complex **3@2** occurs at nearly the same potential as that of the free guest molecule **3**, indicating minimal impact of encapsulation on the initial electron transfer (ET) step. In contrast, the second reduction of **3@2** is irreversible and takes place at a potential 113 mV more negative than the second

reduction of free **3**, suggesting that the guest remains effectively encapsulated after the first reduction, and that the host structure hinders the subsequent ET process. The observed irreversibility likely arises from the release of the guest upon completion of the second reduction. Additionally, the shape of the first reduction wave (process I) for **3@2** is dependent on the scan rate (Fig. 4b). At higher scan rates, peak broadening and a shift to more negative potentials are observed, which can be attributed to the timescale of the measurement becoming comparable to or faster than the molecular dynamics of the system. Under these conditions, a greater fraction of **3@2** remains in its encapsulated form, leading to stronger hindrance of ET to the NDI unit. At slower scan rates, the guest has sufficient time to dissociate from the host, resulting in a reversible redox wave at the same potential as that of process I for both free **3** and **3@2**. A similar effect is observed for process II, which refers to the second ET process. This process is also scan-rate dependent, as the potential becomes more negative at higher scan rates. This is because the scan rate surpasses the  $(3^{\cdot-})@2 \rightarrow 3^{\cdot-} + 2$  conversion, thus leaving  $3^{\cdot-}$  encapsulated during the generation of  $(3^{2-})@2$ .

To assess the affinity of the one-electron-reduced cyclophane  $3^{\cdot-}$  for the metallobox **2**, we performed an experiment where we reduced **3** in  $\text{CD}_2\text{Cl}_2$  by adding one equivalent of cobaltocene. The resulting  $^1\text{H}$  NMR spectrum (Fig. 5b) confirmed the reduction, evidenced by the disappearance of the resonance corresponding to the four equivalent protons of the NDI moiety in **3**. This result strongly suggests that the



**Fig. 4** (a) A comparison of the cyclic voltammograms (CV) of **3** (top) and **3@2** (bottom) (1 mM in  $\text{CH}_2\text{Cl}_2$ , room temperature,  $0.25 \text{ M}$   $[\text{NBu}_4]$   $(\text{PF}_6)$ ,  $100 \text{ mV s}^{-1}$ ). (b) Variable scan rate CVs of **3@2**, showing that the peak potential of processes I, II and IV are scan-rate dependent.



**Fig. 5** Selected region of the NMR spectra ( $\text{CD}_2\text{Cl}_2$ , 500 MHz, 298 K), of (a) **3**, (b) a solution of **3** after addition of one equivalent of cobaltocene, and (c) a solution of **3** + one equivalent cobaltocene + one equivalent of **2**.



reduction of **3** produces a radical species with the unpaired electron localized at the NDI unit, leaving the pyrene moiety largely unaffected. Upon further addition of one equivalent of metallobox **2** (Fig. 5c), the  $^1\text{H}$  NMR spectrum shows a set of resonances consistent with a metallobox that is 'cavity-occupied'. However, the signals for the guest ( $3^{\cdot-}$ ) are no longer visible, and those for the metallobox are significantly broadened compared to the  $3@2$  complex (Fig. 2c). This suggests that the spectrum in Fig. 5c corresponds to the  $(3^{\cdot-})@2$  adduct, with the absence of guest signals and the broadening of metallobox resonances indicating the paramagnetic nature of the host:guest complex. Overall, the experiment confirms the high binding affinity between  $3^{\cdot-}$  and **2**.

The asymmetric nature of the guest suggests the presence of two degenerate orientations in  $3@2$ , as the molecule of **3** can align either of its two distinct planar units (pyrene or NDI) towards the polyaromatic panels of the host (see Fig. 6). This leads to the inequivalence of the resonances of the protons in the polyaromatic ligand at slow exchange rates on the NMR timescale. To investigate this, we conducted a variable-temperature  $^1\text{H}$  NMR experiment in  $\text{CD}_2\text{Cl}_2$ , spanning a temperature range from 20 to  $-40$  °C. As the temperature decreased, the signals corresponding to the aromatic protons of the di-NHC ligand (denoted as **b** and **c** in Fig. 2) became unequivocal, indicating a transition from fast to slow exchange kinetics on the NMR timescale.  $^1\text{H}$  NMR line-shape analysis of the spectra (Fig. 6), with reference to the evolution of the resonances of protons **a** and **a'**, allowed us to determine the rate constants at each temperature. An Eyring plot was used to extract the activation enthalpy ( $\Delta H^\ddagger$ ) and activation entropy



**Fig. 6** Study of the dynamic behavior of  $3@2$  conducted by VT  $^1\text{H}$  NMR spectroscopy. The series of spectra show the region related to the appearance of the resonances **a** and **a'**, as labelled in the reaction scheme. All spectra recorded in  $\text{CD}_2\text{Cl}_2$ . Full spectra are given in the ESI.† The determination of the kinetic constants was performed by dynamic  $^1\text{H}$  NMR line-shape simulations. The simulated spectra (in red) are shown below the experimental ones.

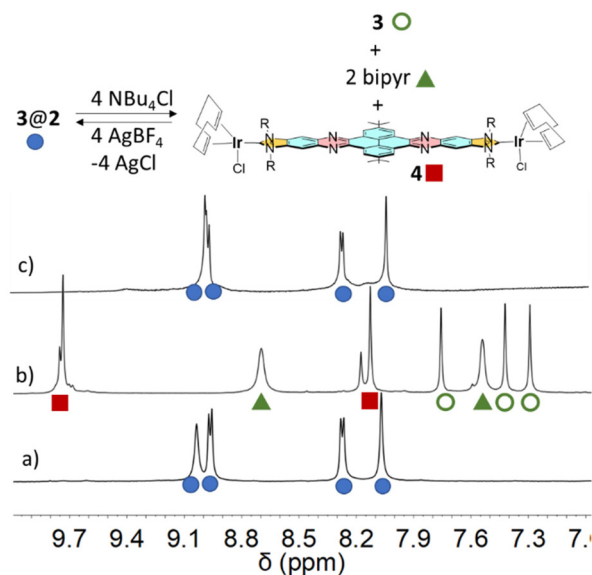


**Fig. 7** Selected region of the NMR spectra ( $\text{CD}_2\text{Cl}_2$ , 500 MHz, 298 K), of  $3@2$  (a), after addition of four equivalents of  $[\text{NBu}_4]\text{Cl}$  (b), and after further addition of four equivalents of  $\text{AgBF}_4$  (c). The resonances of  $3@2$  are represented by solid blue circles, solid green triangles are used of bipyridine, green empty circles for **3**, and red solid squares for **4**.

( $\Delta S^\ddagger$ ), yielding values of  $5.1 \pm 0.2 \text{ kcal mol}^{-1}$  and  $-32 \pm 1 \text{ cal mol}^{-1} \text{ K}^{-1}$ , respectively. These values are consistent with an intermolecular dynamic process, where the guest undergoes a reorientation within the host cavity *via* a dissociative mechanism. The large negative activation entropy suggests that the separate host and guest molecules are more solvateable than the host-guest adduct. The positive activation enthalpy likely reflects the energy cost associated with the structural rearrangements of both the host and the guest during the guest's release.

Finally, we sought to investigate whether the encapsulation of **3** within **2** could be made reversible. The motivation behind this is that the practical application of host:guest supramolecular systems often relies on the establishment of reversible binding mechanisms that allow for the controlled storage and release of cargo in response to a stimulus. We hypothesized that the lability of the pyridine-iridium bond in metallobox **2** could serve this purpose. Indeed, the addition of four equivalents of  $[\text{NBu}_4]\text{Cl}$  to a  $\text{CD}_2\text{Cl}_2$  solution of  $3@2$  led to the release of cyclophane **3**, accompanied by the formation of the NDI-di-NHC connected di-(Ir-Cl) complex **4** (Fig. 7) and free bipyridine. Furthermore, the abstraction of chloro ligands from **4** upon the addition of four equivalents of  $\text{AgBF}_4$  resulted in the re-formation of  $3@2$ , thus demonstrating the reversibility of the guest uptake and release process.

## Conclusions

In summary, we synthesized a pyrene-NDI heterocyclophane that exhibits strong binding affinity with a metallasupramole-



cular assembly composed of a nanosized Janus di-NHC ligand. This high affinity arises from the excellent dimensional matching between the cyclophane and the metallobox cavity. The resulting host–guest complex forms a discrete quadruple stack with alternating D–A–D–D layers, providing an ideal framework for studying electron transfer processes at the molecular level. Electrochemical studies of the free and encapsulated heterocyclophane reveal that encapsulation significantly affects the pyrene–NDI charge transfer process, which is highly dependent on guest uptake and release dynamics. Notably, the reduction of the pyrene–NDI cyclophane generates a radical with an unpaired electron at the NDI unit, which can be stabilized upon encapsulation by the tetracationic metallobox, enhancing its resistance to oxidation. This demonstrates the potential of supramolecular recognition to modulate the redox properties of NDI-based materials and to develop systems with encapsulated, stabilized radicals, which may find applications in molecular electronics and paramagnetic smart materials. To our knowledge, there is only one previous report on a radical NDI being supramolecularly encapsulated and stabilized in a polyaromatic cyclophane.<sup>12</sup>

An intriguing aspect of this host–guest complex is that the guest uptake/release can be controlled by adding chloride anions and silver salts. The introduction of chloride destroys the metallobox, resulting in NDI-di-NHC connected di-(Ir–Cl) and bipyridine, alongside free cyclophane, while the complex can be rebuilt by simply adding soluble silver(I) salts. Studying reversible host–guest interactions is crucial for developing adaptable, efficient, and sustainable systems, as these processes improve reusability, enhance efficiency, and offer valuable insights for designing advanced materials and technologies.<sup>13</sup>

## Author contributions

J. Martínez-Visiedo and S. Ibáñez performed the experimental work. L. Dawe performed the X-ray diffraction studies. E. Peris and S. Ibáñez designed the experiments and supervised the experimental work. All authors have given approval to the final version of the manuscript.

## Conflicts of interest

There are no conflicts to declare.

## Data availability

The datasets supporting this article have been uploaded as part of the ESI.†

## Acknowledgements

We gratefully acknowledge financial support from the Ministerio de Ciencia y Universidades (PID2021-127862NB-I00) and Generalitat Valenciana (CIPROM/2021/079). We are grateful to the Serveis Centrals d'Instrumentació Científica (SCIC-UJI) for providing with spectroscopic facilities.

## References

- (a) Y. J. Jeon, P. K. Bharadwaj, S. W. Choi, J. W. Lee and K. Kim, *Angew. Chem., Int. Ed.*, 2002, **41**, 4474; (b) Y. H. Ko, E. Kim, I. Hwang and K. Kim, *Chem. Commun.*, 2007, 1305; (c) M. Kumar, K. V. Rao and S. J. George, *Phys. Chem. Chem. Phys.*, 2014, **16**, 1300; (d) N. J. Hestand, R. V. Kazantsev, A. S. Weingarten, L. C. Palmer, S. I. Stupp and F. C. Spano, *J. Am. Chem. Soc.*, 2016, **138**, 11762; (e) L. Vallan, E. P. Urriolabeitia, F. Ruipérez, J. M. Matxain, R. Canton-Vitoria, N. Tagmatarchis, A. M. Benito and W. K. Maser, *J. Am. Chem. Soc.*, 2018, **140**, 12862; (f) Y. J. Huang, Z. R. Wang, Z. Chen and Q. C. Zhang, *Angew. Chem., Int. Ed.*, 2019, **58**, 9696; (g) A. A. Dar and S. Rashid, *CrystEngComm*, 2021, **23**, 8007.
- (a) M. D. Gujrati, N. S. S. Kumar, A. S. Brown, B. Captain and J. N. Wilson, *Langmuir*, 2011, **27**, 6554; (b) B. Pramanik, S. Ahmed, N. Singha, B. K. Das, P. Dowari and D. Das, *Langmuir*, 2019, **35**, 478; (c) L. Zeng, L. Huang, Z. H. Wang, J. W. Wei, K. Huang, W. H. Lin, C. Y. Duan and G. Han, *Angew. Chem., Int. Ed.*, 2021, **60**, 23569; (d) S. Barman, S. Bandyopadhyay, A. Ghosh, S. Das, T. Mondal, A. Datta, S. Ghosh and A. Datta, *Chem. Commun.*, 2022, **58**, 10508; (e) A. Mukherjee, S. Barman, A. Ghosh, A. Datta, A. Datta and S. Ghosh, *Angew. Chem., Int. Ed.*, 2022, **61**, e202203817; (f) Z. Y. Huang, Y. H. Weng, Y. F. Yang, B. H. Lin, Y. C. Lin and W. C. Chen, *ACS Photonics*, 2023, **10**, 4509; (g) M. L. Williams, J. R. Palmer, R. M. Young and M. R. Wasielewski, *J. Am. Chem. Soc.*, 2024, **146**, 34130; (h) W. Xu, H. Zhang, Y. Zhou, T. G. Lu, Y. T. Li, Y. X. Zhu, C. Y. Wei, J. T. Zheng, R. H. Li, J. Li, L. J. Chen, G. X. Zhang, J. Shi, J. Y. Liu, D. Q. Zhang and W. J. Hong, *J. Am. Chem. Soc.*, 2025, **147**, 5879.
- (a) S. Burattini, B. W. Greenland, W. Hayes, M. E. Mackay, S. J. Rowan and H. M. Colquhoun, *Chem. Mater.*, 2011, **23**, 6; (b) M. R. Molla and S. Ghosh, *Chem. – Eur. J.*, 2012, **18**, 9860; (c) K. Jalani, M. Kumar and S. J. George, *Chem. Commun.*, 2013, **49**, 5174; (d) A. K. Blackburn, A. C. H. Sue, A. K. Shveyd, D. Cao, A. Tayi, A. Narayanan, B. S. Rolczynski, J. M. Szarko, O. A. Bozdemir, R. Wakabayashi, J. A. Lehrman, B. Kahr, L. X. Chen, M. S. Nassar, S. I. Stupp and J. F. Stoddart, *J. Am. Chem. Soc.*, 2014, **136**, 17224; (e) A. Das and S. Ghosh, *Angew. Chem., Int. Ed.*, 2014, **53**, 1092; (f) S. Bhattacharjee, B. Maiti and S. Bhattacharya, *Nanoscale*, 2016, **8**, 11224; (g) S. Bartocci, J. A. Berrocal, P. Guarracino, M. Grillaud, L. Franco and M. Mba, *Chem. – Eur. J.*, 2018, **24**, 2920;



- (h) F. Peigneguy, C. Oliveras-González, M. Voltz, N. Ibrahim, M. Sallé, N. Avarvari and D. Canevet, *J. Mater. Chem. C*, 2022, **10**, 13989; (i) M. Y. Yeh and H. C. Lin, *Phys. Chem. Chem. Phys.*, 2014, **16**, 24216.
- 4 L. J. Sun, W. G. Zhu, X. T. Zhang, L. Q. Li, H. L. Dong and W. P. Hu, *J. Am. Chem. Soc.*, 2021, **143**, 19243.
- 5 H. Y. Lin, B. J. Zhong, H. J. Liu, Y. K. Wu, C. H. Peng and C. L. Wang, *Cryst. Growth Des.*, 2024, **24**, 2833.
- 6 V. Maurizot, M. Yoshizawa, M. Kawano and M. Fujita, *Dalton Trans.*, 2006, 2750.
- 7 (a) J. K. Klosterman, Y. Yamauchi and M. Fujita, *Chem. Soc. Rev.*, 2009, **38**, 1714; (b) V. Martinez-Agramunt and E. Peris, *Chem. Commun.*, 2019, **55**, 14972; (c) H. T. Tang, Y. Zou, H. N. Zhang and G. X. Jin, *Proc. Natl. Acad. Sci. U. S. A.*, 2025, **122**, e2426356122; (d) X. Y. Wang, Q. S. Mu, X. Gao and G. X. Jin, *Sci. China: Chem.*, 2025, **68**, 1345.
- 8 (a) M. Iwane, T. Tada, T. Osuga, T. Murase, M. Fujita, T. Nishino, M. Kiguchi and S. Fujii, *Chem. Commun.*, 2018, **54**, 12443; (b) Y. Yamauchi, M. Yoshizawa, M. Akita and M. Fujita, *J. Am. Chem. Soc.*, 2010, **132**, 960; (c) T. Murase, K. Otsuka and M. Fujita, *J. Am. Chem. Soc.*, 2010, **132**, 7864; (d) M. Yoshizawa, J. Nakagawa, K. Kurnazawa, M. Nagao, M. Kawano, T. Ozeki and M. Fujita, *Angew. Chem., Int. Ed.*, 2005, **44**, 1810; (e) S. Fujii, T. Tada, Y. Komoto, T. Osuga, T. Murase, M. Fujita and M. Kiguchi, *J. Am. Chem. Soc.*, 2015, **137**, 5939; (f) N. Singh, J. H. Jo, Y. H. Song, H. Kim, D. Kim, M. S. Lah and K. W. Chi, *Chem. Commun.*, 2015, **51**, 4492.
- 9 S. Ibáñez, P. Salvà, L. N. Dawe and E. Peris, *Angew. Chem., Int. Ed.*, 2024, **63**, e202318829.
- 10 S. Ibáñez and E. Peris, *Inorg. Chem.*, 2024, **63**, 16070.
- 11 (a) P. Thordarson, *Chem. Soc. Rev.*, 2011, **40**, 1305; (b) A. J. Lowe, F. M. Pfeffer and P. Thordarson, *Supramol. Chem.*, 2012, **24**, 585.
- 12 T. Jiao, K. Cai, J. N. Nelson, Y. Jiao, Y. Qiu, G. Wu, J. Zhou, C. Cheng, D. Shen, Y. Feng, Z. Liu, M. R. Wasielewski, J. F. Stoddart and H. Li, *J. Am. Chem. Soc.*, 2019, **141**, 16915.
- 13 T. Y. Kim, R. A. S. Vasdev, D. Preston and J. D. Crowley, *Chem. – Eur. J.*, 2018, **24**, 14878.

